ORIGINAL PAPER

How highly efficient power electronics transfers high electrocaloric material performance to heat pump systems

Stefan Mönch[1] · Richard Reiner[1] · Patrick Waltereit[1] · Michael Basler[1] · Rüdiger Quay[1] · Sylvia Gebhardt[2] · Christian Molin[2] · David Bach[3] · Roland Binninger[3] · Kilian Bartholomé[3]

Abstract

Electrocaloric heat pumps for cooling or heating are an emerging emission-free technology, which could replace vapor-compression systems, harmful refrigerants, and mechanical compressors by a solid-state solution with theoretically even higher coefficient of performance. Existing electrocaloric ceramics could reach around 85% of the Carnot-limit, and existing electrocaloric polymers could enable a compact and high power density system. However, the performance of published system demonstrators stays significantly below this performance, partly because of the external electronic charging loss (cyclic charging/discharging of electrocaloric capacitors). This work analyzes how the latest 99.74% ultra-efficient power electronics enables to maintain a high performance even at the system level. A first-principle analysis on material and system parameters also shows the effect of significantly different material properties of ceramics (PMN, PST) and PVDF-based polymers on system parameters. A system benchmark provides insight into system characteristics not covered by material analysis.

Introduction

Electrocaloric heat pumps offer cooling and heating with zero global warming potential [1]. While some known electrocaloric materials (ceramics [2], polymers [3]) could outperform vapor-compression systems [4, 5], published demonstrators still have significantly lower performance. This is partly due to losses from the charging electronics, required to cyclically charge/discharge the electrocaloric capacitors. This paper discusses latest research of ultra-efficient power electronics, and how it enables to transfer the high material performance to the system level.

✉ Stefan Mönch
stefan.moench@iaf.fraunhofer.de

✉ Sylvia Gebhardt
sylvia.gebhardt@ikts.fraunhofer.de

✉ Kilian Bartholomé
kilian.bartholome@ipm.fraunhofer.de

[1] Fraunhofer Institute for Applied Solid State Physics IAF, 79108 Freiburg, Germany

[2] Fraunhofer Institute for Ceramic Technologies and Systems IKTS, 01277 Dresden, Germany

[3] Fraunhofer Institute for Physical Measurement Techniques IPM, 79110 Freiburg, Germany

Methods

Material and system coefficient of performance (COP) limits

The achievable material COP relative to the ideal Carnot-COP, called relative material COP in the following,

$$COP_{R,MAT} \approx \frac{1}{1 + \frac{1}{\alpha}\frac{1}{FOM}} = \frac{1}{1 + \frac{1}{\alpha}\underbrace{\frac{\varepsilon_{TR}T\Delta E^2}{\rho c_P \Delta T_{AD}^2}(\frac{\pi}{4}DF_{TR})}_{=\frac{1}{FOM}=\frac{\Delta T_{HYST}}{\Delta T_{AD}}}}, \quad (1)$$

is below the limit $COP_R = 1 = 100\%$ due to non-reversible dielectric (hysteresis) loss, where $\alpha = 1/4$ for Carnot-like cycles, or up to $\alpha = 1$ for cycles with temperature regeneration by ΔT_{AD}. The term "Carnot-like" is used in this work to describe a thermal cycle in a system without heat regeneration, where half of the electrocaloric temperature change is used to actively overcome the temperature difference in each stage, and only the remaining half is then available for useful cooling/heating. Furthermore, the term "Carnot-like" is used to state that the heat flow from the electrocaloric element to the sink/source (or next/previous stage) is approximately iso-thermal, and thus the most efficient heat transfer, compared

to for example Brayton cycles. Details on this Carnot-like cycles for electrocaloric systems are discussed for example in [6–9]. *FOM* is a material figure-of-merit from [9] (the ratio of reversible temperature change ΔT_{AD} to non-reversible temperature change ΔT_{HYST} during one adiabatic cycle), similar to analyses in [6, 10, 11] based on the equivalent permittivity ε_{TR} and dissipation factor DF_{TR} of the electrocaloric dielectric (which condense the voltage-dependent permittivity and dissipation factor each into just one equivalent value, as described in [6]) with density ρ and heat capacity c_{P}, operation temperature T, and the electric field change ΔE which causes an electrocaloric and adiabatic temperature change of ΔT_{AD}. The dissipative heat per cycle and volume (see also [9, 12]) can be calculated from the electrical equivalent values as $q_{\text{DISS}} = \frac{\pi \varepsilon_{\text{TR}} \Delta E^2 DF_{\text{TR}}}{4\rho}$. The dissipation factor can also be expressed as a loss tangent $\tan(\delta) = DF_{\text{TR}}$ which is typically used for sinusoidal signals. However, to condense the non-linear capacitance and loss data to just one equivalent value each, this work uses a dissipation factor to emphasize the ratio of dissipative electrical energy to stored energy which is also well-defined for non-sinusoidal signals. Possible origins for the dissipative heat in (electrocaloric) dielectrics are for example dipole relaxation [13], domain wall motion [14], defects [15] or molecular chain dynamics [16] (in polymers), and these effects are temperature, electrical field and frequency dependent. Only the hysteresis loss is considered here as an equivalent time-related dissipation factor, and series-resistances and leakage current related losses can be neglected if the system frequency is carefully selected. The system frequency should be sufficiently high that the static (independent from system frequency) leakage current related power loss is much smaller than the dynamic (proportional to system frequency) hysteresis loss. At the same time, the system frequency (proportional to the charging current) should be sufficiently low such that series-resistance losses not yet dominate the hysteresis losses. The frequency where the series-resistance losses starts to dominate can be adjusted (and thus increased) by changing the geometry or material of the electrodes.

Several materials with high FOMs exist, for example lead magnesium niobate (PMN), lead scandium tantalate (PST), or barium titanate (BT)-based ceramics and polyvinylidene fluoride (PVDF)-based (ter-)polymers. However, such high system COPs have not yet be reached, because the external charging circuit loss reduces $COP_{\text{R,MAT}}$ to the lower relative system COP

$$COP_{\text{R,SYS}} \approx \frac{1}{1 + \frac{1}{\alpha} \underbrace{\frac{\varepsilon_{\text{TR}} T \Delta E_{\text{MAX}}^2}{\rho c_{\text{P}} \Delta T_{\text{AD,MAX}}^2} (\frac{\pi}{4} DF_{\text{TR}} + (1 - \eta_{\text{DC}}))}_{\underbrace{(4FOM_{\text{EC}})^{-1}}_{FOM^{-1} = (4FOM_{\text{EC,MAT}})^{-1}}}},$$

(2)

with a material figure-of-merit FOM_{EC} [6] independent from DF_{TR} (the factor $\frac{\pi}{4}$ is justified in [6]), and non-ideal charging efficiency $\eta_{\text{DC}} < 100\%$. The material figure-of-merit $FOM_{\text{EC,MAT}}$ [6] which includes the material's dissipative loss was adapted in [9] to an improved figure-of-merit $FOM = 4FOM_{\text{EC,MAT}}$ which does not include the factor of four any more, because it is now included as a factor α independent from *FOM*. The factor of four related to the thermal cycle is also discussed in [8, 9, 17]. Eqn. 2 shows that the charging circuit loss $(1 - \eta_{\text{DC}})$ reduces the system COP additionally and similarly as *DF*. Rearranging Eqn. 2 as

$$COP_{\text{R,SYS}} \approx \frac{1}{1 + \frac{1}{\alpha} \frac{1}{FOM} \left(1 + \frac{1 - \eta_{\text{DC}}}{\frac{\pi}{4} DF_{\text{TR}}}\right)},$$

(3)

highlights that a high material *FOM* is not sufficient, but also a high efficiency η_{DC} in relation to DF_{TR} is required for systems. For the material *FOM* only the product $\varepsilon_{\text{TR}} DF_{\text{TR}}$ is relevant, but for systems the trade-off between ε_{TR} and DF_{TR} becomes important, which was noticed in [6]. For two materials with the same *FOM* (same material COP limit) and given charging efficiency η_{DC}, it is easier to achieve a high system performance, if the permittivity is reduced in a trade-off for DF_{TR}.

In any case, a high electrical charging efficiency is required [2] to transfer the high material performance to the system level, which motivates research on charge recovery circuits for electrocalorics.

Ultra-efficient power electronics as charge recovery circuit

In 2018, E. Defay et al. [18] proposed the charge recovery by a resonant circuit for electrocalorics, demonstrating up to 86% efficiency, charging ceramic capacitors in a system demonstrator. In 2020, Meng et al. [19] used a resonant circuit for a polymer-based system, reporting efficiencies of 70% and a measured $COP_{\text{R,SYS}} = 12\%$, the highest measured electrocaloric system COP known to the authors, which, however, is still significantly below the material limit. As stated in the supplementary materials of [19], the prototype which achieved $COP_{\text{R,SYS}} = 12\%$ used polymer material with a performance limit which is below other published polymer data (e.g. [20]), such that that system performance is

limited not only by the charge recovery efficiency of the used resonant-circuit, but also by the material and the thermal cycle (Brayton without heat regeneration). In the supplementary materials of [19], a relative system performance of 44% is predicted if an improved polymer material was used. In 2022, M. Almanza et al. [17] used a Marx modulator for electroactive polymers and reported charging efficiencies of 88%. In 2022, Moench et al. [6] proposed to use a switched-mode power electronics approach, achieving 99.2% efficiency. In 2023, S. Mönch et al. [21] demonstrated a partial power processing power electronics shown in Fig. 1 with 99.74% efficiency, continuously charging/discharging 10 µF by 317 V at 19 Hz. This circuit only has 0.26% losses, a 50-times reduction compared to the initial resonant circuit approaches previously used for electrocaloric demonstrators. Application of such highly-efficient electronics to electrocaloric heat pump demonstrators will significantly improve the system COP, and could also enhance electrocaloric energy harvesting [22].

In [6] an electrocaloric PMN ceramic fabricated as in [23] by the authors from Fraunhofer IKTS, was measured, and driven with offset voltages. Offsets avoid the high permittivity at low voltages, as observed in [18], resulting in a calculated $FOM = 28.6$, low $DF_{TR} = 0.06\%$ and high $COP_{R,MAT} \approx 87.7\%$ for Carnot-like cycles [6].

The predicted system performance however was reduced to 28.6% when using the 99.2% efficient electronics [6], and it was calculated that $\eta_{DC} \geq 99.71\%$ is needed to maintain at least $COP_{R,SYS} \geq 50\%$ (Carnot-like cycles). The 99.74% efficient converter from [21] thus is now sufficiently efficient and marks a milestone to transfer high material COPs to the heat pump system performance.

Carnot-like cycles using field variation

The thermal cycle influences the heat pump performance. Demonstrators (reviews: [24, 25]) typically use Brayton-cycles, less efficient [7] than the previously analyzed Carnot-like cycles. Initial resonant circuits [18, 19] allowed energy recovery, but only square-like voltage waveforms (with sinusoidal-like transitions), resulting in Brayton-cycles.

The power electronics approach now also allows arbitrary voltage variation, for example four-step voltage waveforms (the charging and discharging transitions are split into a fast and slow half) for Carnot-like cycles, experimentally demonstrated in [26] with a two-stage cascaded system demonstrator, inspired by [18, 27]. Since the power electronics approach (compared to a resonant circuit) decouples the charging time from the inductor value and electrocaloric load capacitance, it allows varying charging/discharging speeds by burst-mode operation within one cycle. This burst-mode operation has additional switching transitions from standby-phases (between the bursts) and the standby-phases cause the static leakage currents to contribute more to the total losses. A 10:1 charging speed ratio reduced the measured charging efficiency slightly from 99.2% to 98.9% in [26]. Advanced circuit topologies could solve this issue, for example by multi-phase charging of several individual EC loads with just one converter, such that the converter is operated all the time (zero standby phases), and the individual EC loads are connected and disconnected several times as needed during each cycle. Otherwise, the slightly reduced charging efficiency will reduce the system COP slightly, according to Eq. 3 (also visible in the later presented Fig. 3. It is estimated that the slight reduction of charging efficiency due to the burst-mode operation for Carnot-like cycles still

Fig. 1 99.74% efficient partial-power processing charging circuit for electrocaloric capacitive loads. Figure from [21]
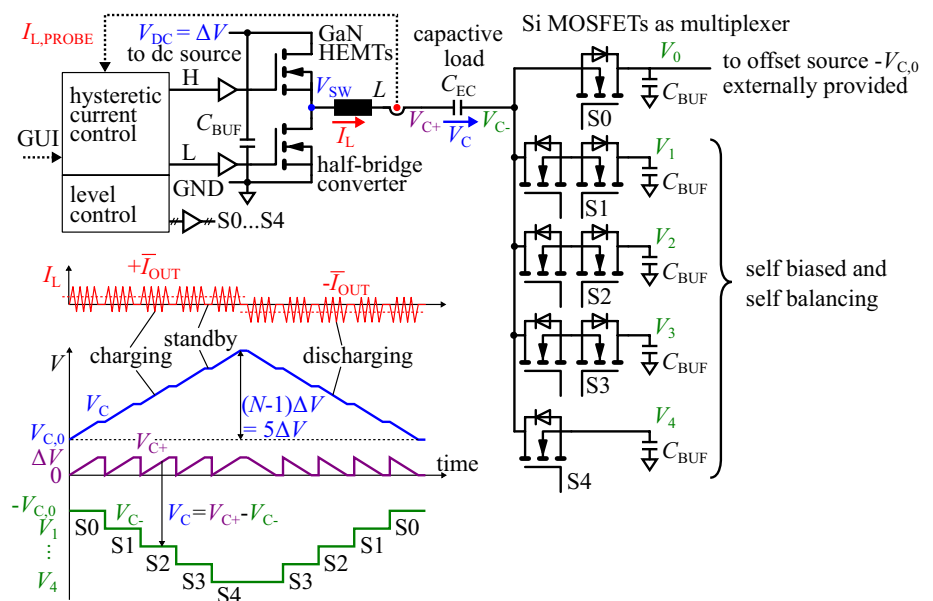
results in a higher system COP than for a Brayton-cycle (compared in [7]) where the burst-mode operation is not required (maximum electrical charging efficiency). In the meantime, a ten-stage demonstrator was built, shown in Fig. 2, demonstrating scalability.

Results and discussion

Material and system benchmarking

The effect of material and system parameters on COP is analyzed for three materials (four cases): (1) PMN ceramic [6] fabricated by Fraunhofer IKTS, with offset E_0 and (2) without; data from [6]. (3) PST ceramic [28] MLCC [29] by Hirose (muRata); measured data by the authors. The selected operation point is at a slightly elevated temperature, where the hysteresis loss is significantly reduced, while the measured adiabatic temperature change is only slightly reduced from the measured maximum at the same electric fields but lower temperature, resulting in an better material performance (the optimal material performance is not necessary at the temperature of maximum adiabatic temperature change). (4) PVDF-based terpolymer by Qian; data from [20].

The authors clearly state that this work primarily is a guidance to benchmark electrocaloric systems in general, but the selected materials and operation points are just an example snapshot. Other and improved materials, and operation conditions were published and are part of ongoing research. For example, PMN data by Plaznik [2] could result in even higher performance. PST could be operated at higher fields [29, 30], improving the power density but possibly also reducing the coefficient of performance because the gain of additional electrocaloric temperature change might be lower than the additionally required electrical charging power (and associated losses) [30]. Increased B-site ordering [29] will further increase the adiabatic temperature change and performance. Also, lead-free ceramics are researched [31, 32]. PVDF-based nanoparticle-filled composite polymer-based materials [33] and hysteresis reduction is currently researched, improving the performance. This work aims for a general performance benchmark and method, also unveiling system level parameters often overlooked and not covered by pure material characterization.

This work neglects that the thermal connections in the cascade have to be practically realized with some system approach, and also neglects that the actuation and additional thermal resistance and capacitance of these connections can limit the achievable system frequency and also can reduce the system performance compared to the simplified calculations used in this work. Several thermal control devices are reviewed in [34]. The high system frequency of 10 Hz assumed in this work seems possible because up to 20 Hz was predicted using simulations for a thermal switch capacitor in [35] and for a ferrofluidic thermal switch in [36]. A high frequency of 20 Hz using mechanical check valves in a magnetocaloric heat pipe heat pump was experimentally achieved in [37]. Even though such check valves in a heat pipe-based heat pump system are opened and closed by the pressure change in the heat pipe, and thus do not have to be actively controlled, there will still be a non-zero pressure drop (or temperature drop) in each stage related to the minimum opening pressure, possibly reducing the system performance. Also, thermal switches typically have a low thermal contrast ratio (investigated for example in [38]), because typically also in the off state of the thermal switch there exist parallel heat flow paths through the mechanical structure, limiting reducing the useful cooling/heating power.

For simplicity, this work assumes the same material performance as from one measured temperature point over the complete heat pump temperature range, even though it is well known that the usable temperature range of some electrocaloric materials is limited. The limited temperature range of some electrocaloric materials is not considered in this work, such that the calculated relative performance of the benchmark system (with a large temperature span) is the same as that of just one individual stage with low temperature span. In [39] the temperature span where the electrocaloric effect maintains 90% of the maximum ΔT_{AD} is discussed for several electrocaloric materials.

Table 1 lists extracted and calculated material and system parameters for a benchmark heat pump systems (cooling with cold site temperature T). As benchmark system a cascaded heat pump was selected because it allows high

Fig. 2 Ten-stage electrocaloric heat pump demonstrator

BaTiO3
MLCCs
20ct/pc

5cm
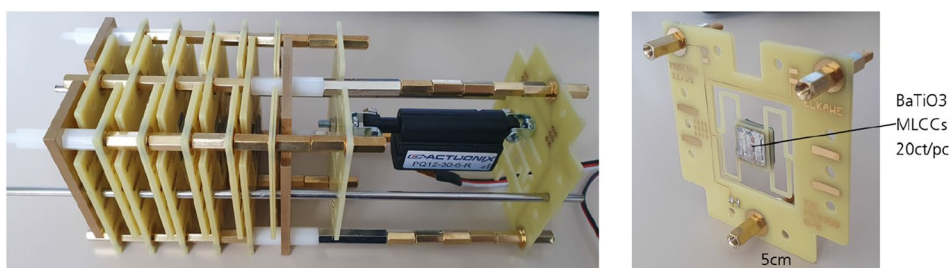
system frequencies [37]. However, so far only simple cascades without heat regeneration have been demonstrated. Therefore, a Carnot-like cycle ($\alpha = 1/4$) is selected as reference case. From the time-related, large-signal permittivity ε_{TR} and dissipation factor DF_{TR}, the adiabatic temperature change ΔT_{AD} (at electric field change ΔE on top of the offset E_0), the heat capacity c_P and density ρ of the electrocaloric material, and the figure-of-merit FOM are calculated. The material's relative COP limit $COP_{R,SYS}$ is calculated from Eq. 1 for a Carnot-like cycle ($\alpha = \frac{1}{4}$), and for an ideal regenerative cycle ($\alpha = 1$). The available entropy change $\Delta S_{ISO,MAX} \approx \frac{\Delta T_{AD}}{T} c_P$ is estimated, and the thermal hysteresis ΔT_{HYST} follows from FOM and Eq. 1. The non-reversible dissipation $q_{DISS} \approx \Delta T_{AD} \Delta S_{ISO,MAX} FOM^{-1}$ is estimated from DF_{TR}. It should be mentioned that only the hysteresis loss related to DF_{TR} is considered in the calculations. It was assumed that leakage current losses and series-resistance losses are negligible compared to the hysteresis loss. While for the investigated PMN and PST MLCCs this assumption is justified, for polymers a more detailed analysis should be carried out based on measured leakage currents.

As benchmark system, a heat pump with $P_{TH,C} = 1 \text{ kW}$ thermal cooling power, $T_{SPAN} = 30 \text{ K}$ temperature span, and $f_{SYS} = 10 \text{ Hz}$ system frequency (feasible if a heat-pipe system approach from magnetocalorics [37] is adapted to electrocalorics).

A factor α is used to describe the thermal cycle and additional heat regeneration, e.g. $\alpha = 1/4$ for Carnot-like cycles in a simple cascade without heat regeneration (half the adiabatic temperature change is used to overcome the optimal temperature difference per stage, and then only half of the thermal energy is available for cooling/heating, thus a factor of 4), or $\alpha = 1$ for a system with heat regeneration where a temperature change of ΔT_{AD} per stage is overcome by an additional heat regenerator, which is twice that of a Carnot-like cycle, and the full (twice compared to the Carnot-like cycle) thermal energy from the electrocaloric effect is then still available for cooling/heating. An example for such a heat regeneration system in an electrocaloric system is found for example in [40].

In addition to relative system parameters (such as the relative material and system COPs from Eqs. 1–3) which are independent from the actual sizing of a heat pump (at least within the simplifications used by his work), some further absolute system parameters are also calculated, which enables an assessment of whether such a system could be realized in practice with justifiable use of materials: For a Carnot-like cycle ($\alpha = 1/4$), a number of $N_{CASC} = 2\frac{T_{SPAN}}{\Delta T_{AD}}$ series-cascaded stages is required because the electrocaloric temperature change of known material is smaller than the desired heat pump temperature span ($\Delta T_{AD} \ll T_{SPAN}$). The compactness depends on the active electrocaloric volume $\Upsilon = 2\frac{N_{CASC}P_{TH,C}}{f_{SYS}\Delta T_{AD}\rho c_P}$ (equivalent cube-length: $l_\Upsilon = \sqrt[3]{\Upsilon}$) and weight $m = \rho\Upsilon$. The average charging power $P_{CHARGE} = \varepsilon_0\varepsilon_{TR}\Delta E^2\Upsilon f_{SYS}$, cycling within the system, depends on the permittivity. Exemplary for $V = 400 \text{ V}$ operation voltage (typical for single-phase electronics) the equivalent capacitance $C = \varepsilon_0\varepsilon_{TR}\left(\frac{\Delta E}{V}\right)^2\Upsilon$ is calculated. In this work an operation voltage of $V = 400 \text{ V}$ was arbitrarily chosen, because high electrical charging efficiencies of 99.2% and 99.74% (used for later system calculations) were achieved in [6] and [21] (for ideal almost lossless non-electrocaloric reference capacitors) with 600 V transistors, which have typical operation voltages around $V = 400 \text{ V}$. Also, a 400 V dc voltage can be efficiently generated by power-factor-correction circuits (e.g. bridgeless totem-pole PFC) from the typical ac grid voltage of up to 230 V) Furthermore, for the ceramic materials investigated, the required electrical fields in combination with the permittivity of the electrocaloric material lead to typical layer thicknesses of several 10 s of micrometers if dimensioned for 400 V, which is a feasible layer thickness for MLCC fabrication. For example, PST-based MLCCs published in [29] use 38 µm layer thickness, such that the electric field from the electronics can provide up to 10 V/µm, sufficient to cause the electrical fields for ceramics considered in this work. For polymers with higher electric fields, either thinner films should be used, or the power electronics has to be dimensioned for a higher operation voltage, either by using higher-voltage transistors (e.g. 1.2 kV or 1.7 kV), or by using advanced circuit topologies (e.g. high-voltage modular multilevel converters other Marx-generators [17]). The average charging current is $I_{CHARGE} = P_{CHARGE}/V$ (continuous charging waveforms), and is possibly increased to higher peak charging currents if standby-phases (current reduced to zero) are used during heat transfer. The stored electrical energy $W_{STORE} = \frac{1}{2}\varepsilon_0\varepsilon_{TR}(E_0 + \Delta E)^2\Upsilon$ within the system is significantly higher than the thermal energies per cycle. All previous characteristics are reduced (halved) if regenerative cycles are used ($\alpha = 1$).

For selected charging efficiencies η_{DC} (0%: no recovery, 50%: as in resistive charging, 99.2%: conventional power electronics, 99.74% ultra-efficient power electronics), the best-case $COP_{R,SYS}$ is calculated (Carnot-like and regenerative cycles).

For practical considerations, the absolute COP is also evaluated, to compare to the Carnot limit COP_{CAR}.

Table 1 Calculated material, system and heat-pump (cooling) benchmark system parameters

			PMN	PMN (offset)	PST	Polymer
Temperature (cold)	T	[K]	300	300	312.52	300
Rel. permittivity	$\varepsilon_{TR}/\varepsilon_0$	[1]	4000	725	4827	53
Density	ρ	[kg/m^3]	7950	7950	8750	1800
Heat capacity	c_P	[J/kg/K]	326	326	308	1500
Electric field change	ΔE	[V/μm]	8	2	5.26	50
Electric offset field	E_0	[V/μm]	0	6	0.00	0
Adiabatic temp. change	ΔT	[K]	1.138	0.2	1.74	8
Dissipation factor	DF_{TR}	[1]	0.16%	0.06%	0.76%	9.15%
Figure-of-merit	FOM	[1]	3.93	28.56	3.68	6.83
Material limit ($\alpha = \frac{1}{4}$)	$COP_{R,MAT}$	[1]	49.5%	87.7%	47.9%	63.1%
Material limit ($\alpha = 1$)	$COP_{R,MAT}$	[1]	79.7%	96.6%	78.6%	87.2%
Max. entropy change	$\Delta S_{ISO,MAX}$	[J/kgK]	1.24	0.22	1.71	40.00
Thermal hysteresis	ΔT_{HYST}	[K]	0.290	0.007	0.473	1.171
Disspation density	q_{DISS}	[J/kg]	0.358	0.002	0.812	46.837
			Benchmark system			
Cooling power	$P_{TH,C}$	[W]	1000			
Temperature span	T_{SPAN}	[K]	30			
System frequency	f_{SYS}	[Hz]	10			
			Evaluation of benchmark system for Carnot-like cycle $COP_{R,SYS}(\alpha = \frac{1}{4})$			
No. of stages (cascade)	N_{CASC}	[1]	52.7	300.0	34.5	7.5
Volume (EC material)	Υ	[m^3]	0.003575	0.115754	0.001471	0.000069
Length of cube (EC mat.)	l_Υ	[m]	0.153	0.487	0.114	0.041
Weight (EC mat.)	m	[kg]	28.42	920.25	12.87	0.13
Electr. charging power	P_{CHARGE}	[W]	81040	29722	17412	815
Elec. capacitance	C(400 V)	[F]	0.05065	0.01858	0.01088	0.00051
Charging current	I_{CHARGE}	[A]	202.6	74.3	43.5	2.0
Stored energy in C	W_{STORE}	[J]	4052	23778	871	41
			Rel. system COP, Carnot-like cycle $COP_{R,SYS}(\alpha = \frac{1}{4})$ [1]			
Rel. $COP_{R,SYS}$	$\eta_{DC} = 0\%$		0.1%	0.3%	0.5%	10.3%
	$\eta_{DC} = 50\%$		0.2%	0.7%	1.1%	17.7%
	$\eta_{DC} = 99.2\%$		11.8%	28.4%	28.3%	60.6%
	$\eta_{DC} = 99.74\%$		24.2%	52.3%	39.1%	62.2%
Abs. COP_{SYS}	$\eta_{DC} = 99.74\%$	[1]	2.4	5.2	4.1	6.2
			Rel. system COP, regeneration-cycle $COP_{R,SYS}(\alpha = 1)$ [1]			
Rel. $COP_{R,SYS}$	$\eta_{DC} = 0\%$		0.5%	1.3%	2.1%	31.4%
	$\eta_{DC} = 50\%$		1.0%	2.6%	4.2%	46.2%
	$\eta_{DC} = 99.2\%$		34.8%	61.4%	61.2%	86.0%
	$\eta_{DC} = 99.74\%$		56.1%	81.4%	71.9%	86.8%
Abs. COP_{SYS}	$\eta_{DC} = 99.74\%$	[1]	5.6	8.1	7.5	8.7
Carnot limit	Abs. COP_{CAR}	[1]	10	10	10.4	10
Data source			[6]	[6]	[9, 29 and own meas.]	[20]

Discussion of benchmark results

Offset fields (PMN ceramic)

Comparing PMN without and with offset (here 75% of a common maximum field) shows that the offset improves the *COP*. Using just the 99.74% efficient power electronics, but no offset fields, and Carnot-like cycles, only a $COP_{R,SYS} \approx 24.2\%$ is predicted. Only when using the offset, the analyzed PMN reaches an improved (doubled) system COP of 52.3%. The offset reduces the material utilization. While the average permittivity ε_{TR} and dissipation factor

DF_{TR} are both reduced, reducing the required charging power (from 81 kW to 29.7 kW) and current (from 203 A to 74 A), the required mass/volume is significantly increased (32-times, from 28 kg to 920 kg), because more elements have to be cascaded. The offset also increases the stored energy (6-times, from 4 kJ to 24 kJ).

The use of offset fields is analyzed here only for the PMN ceramic, which is known to have a very non-linear capacitance-voltage characteristic. In literature, a similar improvement was demonstrated for BT-based materials [18]. Other materials, including other ceramics, and especially also polymers, could also be analyzed with respect to offset fields, but are not expected to yield such high improvements due to other dielectric properties.

This work investigates the effect of offset fields only for PMN ceramics where such data is available in literature. The effect of offset fields for other electrocaloric materials (PST ceramic, polymers,...) should be investigated in future works.

Choice of material

When comparing PST and PMN (without offset) ceramics, both have similar material performance limits $COP_{\mathrm{R,MAT}} \approx 50\%$. However, on the system level the PST ceramic is beneficial because of a higher ΔT_{AD} per stage, and higher DF_{TR} despite similar $COP_{\mathrm{R,MAT}}$, making it easier to reach high system COPs with the same external charging efficiency.

With PST, compared to PMN, only around half the material is required. Also the charging power is reduced to around a fifth. The calculated 17 kW electrical charging power seem still practically feasible for a 1 kW heat pump. Due to the different material parameters a higher system COP is reached. Here, with the 99.74% efficient electronics, a $COP_{\mathrm{R,SYS}} \approx 39.1\%$ is predicted for Carnot-like cycles.

The properties of polymers fundamentally differ from ceramics, for example up to 100-times lower $\varepsilon_{\mathrm{TR}}$, but 10 to 100-times higher DF_{TR}, and high adiabatic temperature changes were reported. Nevertheless, the material limit ($COP_{\mathrm{R,SYS}} \approx 63\%$ for Carnot-like cycles) of the polymers is surprisingly still similar to the ceramics without offset, and even lower than PMN with offset. However, on the system level other improved system parameters follow: The required mass/volume of the polymer is much lower (up to 100-times). Lower requirements for the electronics follow: Only 8 cascaded stages are sufficient (30-300 with the ceramics), and a mass of 0.13 kg. The reactive charging power 815 W (charging current 2 A) is now well-balanced to the thermal power. The stored energy is also significantly reduced. The sensitivity on the electrical charging efficiency is low, a conventional 99.2% efficient electronics is sufficient to reach $COP_{\mathrm{R,SYS}} \geq 60.6\%$ close to the material limit.

A high number of cascaded stages is not desired, because each stage requires thermal valves, complicating the system and possibly leading to lower system reliability due to the increased number of parts. While this work carries out a best-case analysis, in real systems there might be a minimum absolute temperature (or pressure) drop per stage reducing the material performance, which is more significant if the temperature (or pressure) change per stage is low. In a real system, such a constant temperature drop results because at least a small temperature difference between the electrocaloric element and heat sink/source is required for heat transfer (a true isothermal heat transfer would mean infinitely slow cycle times and thus very low power density). In a heat pipe heat pump system, a small pressure drop can result from the operation principle of passive check valves [37]. Nevertheless, a high number of stages (several 10 s to 100 s) could in general be engineered in a system. In other domains (e.g. electrical) cascading of many stages is also successfully used, for example series-connecting 100 s of low-voltage battery-, fuel- or photovoltaic-cells to high voltage systems.

Electrical charging power requirement within the system

For a given thermal power, the material volume is inversely linked to the cycle frequency ($\Upsilon \sim \frac{1}{f_{\mathrm{SYS}}}$). Increasing cycle frequency thus reduces the required material. However, the average electrical charging power is not linked to the cycle frequency. A doubling of cycle frequency halves the required material, but this has to be charged twice as often, not reducing the charging power. This means, that increasing the frequency does not reduce the size (mass and cost) of the electronics. The relation between the reactive charging power (within the system boundaries) and the thermal power is estimated as $\frac{P_{\mathrm{CHARGE}}}{P_{\mathrm{TH,C}}} \approx \frac{1}{\alpha} \frac{T_{\mathrm{SPAN}}}{\Delta T_{\mathrm{AD}}} \frac{\varepsilon_0 \varepsilon_{\mathrm{TR}} \Delta E^2}{\Delta T_{\mathrm{AD}} \rho c_{\mathrm{P}}}$, which is the ratio of electrical energy storage density to thermal electrocaloric heat density, multiplied by the required number of cascade stages and a factor for the thermal cycle. Compared to the $COP \approx \frac{P_{\mathrm{TH,C}}}{P_{\mathrm{EL,IN}}}$ which only describes the COP observed at the system boundaries, the approximate ratio $\frac{P_{\mathrm{CHARGE}}}{P_{\mathrm{TH,C}}}$ describes how much reactive charging power has to be provided within the system compared to the thermal cooling power. From this considerations it directly follows that materials with very low dissipation factor but similar *FOM* require very high electrical charging powers within the system, even if outside the system boundaries this is not visible from the thermal power and electrical (loss) input power.

Hazardous stored electrical energy

The stored energy in the electrocaloric capacitors is a possible hazard. Eletrocaloric capacitors are designed to have

MRS 🕭 Springer
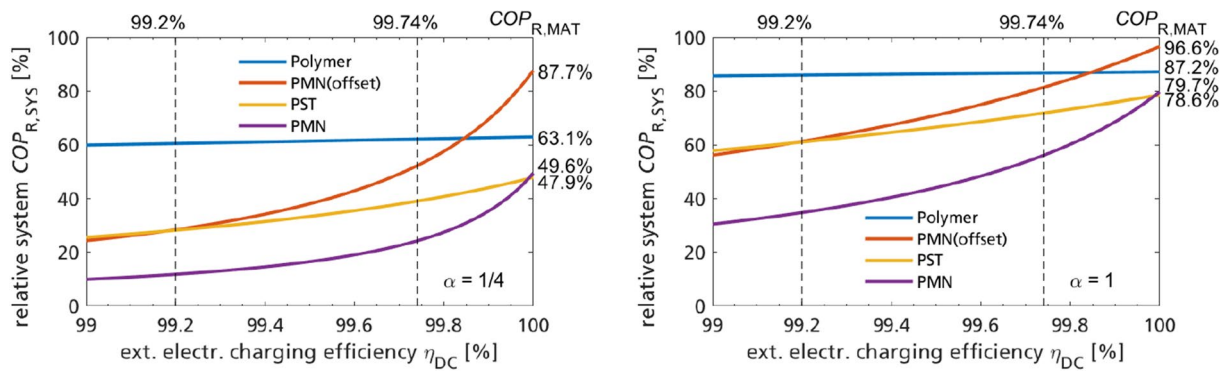
Fig. 3 Best-case system COP as a function of external electrical charging efficiency for different materials and for a Carnot-like cycle and a regenerative cycle

negligible series resistance and high pulse current capability, which allows rapid discharge of the complete stored energy. The stored energy in the range of 41 J (polymer) to over 20 kJ (ceramic with offset), is beyond the energy limit of 1 J [41] typically considered as a threshold at 400 V operation voltage, before serious shock injuries are expected, in case the energy is accidentally discharged through a human. System-level safety and protection measures are thus required. However, they seem manageable, compared to the risk of refrigerants (harmful to the environment) in conventional vapor-compression heat pumps which is technically less manageable.

Choice of thermal cycle

The thermal cycle (Carnot-like, Brayton, Ericsson, Otto,...) influences the system performance, but, since it is a universal approach not limited to electrocalorics, it is only briefly discussed. Most electrocaloric system demonstrators use less efficient Brayton-cycles. A more efficient Carnot-like cycle can be realized for example by a two-step voltage waveform as previously discussed. Thermal regeneration can further improve the performance. Exemplary, temperature regeneration of ΔT_{AD} per stage is considered as a regenerative cycle, such that the full field and electrocaloric entropy change is still available on the hot/cold site (factor $\alpha = 1$ or 1/4 in the analysis). Such a regenerative cycle can be realized for example by a rotary solid-to-solid heat exchanger as in [40]. The effect of systems with no heat regeneration (simple cascade) and ideal regeneration (ideal regenerator) is analyzed in [9] using figure-of-merits and described in more detail.

For a regenerative cycle with the 99.74% efficient electronics, a $COP_{R,SYS} \approx 72\% - 87\%$ is predicted in Table 1.

Effect of charging efficiency on system performance for different materials

Figure 3 plots the best-case $COP_{R,SYS}$ depending on charging efficiency η_{DC} (Eq. 2, data from Table 1).

The different sensitivity of $COP_{R,SYS}$ from η_{DC}, when comparing ceramics and polymers, cannot be explained only by the material FOM, but depends on the ratio between ε_{TR} and DF_{TR}. Two materials with same FOM, and consequently the same material limit $COP_{R,MAT}$, can still show significantly different system performance for $\eta_{DC} < 100\%$. Especially if ε_{TR} is very high and DF_{TR} very low (e.g. $< 0.1\%$ such as in PMN ceramics, and $DF_{TR} \ll (1 - \eta_{DC})$, then on the system level now the product $\varepsilon_{TR}(1 - \eta_{DC})$, and the external charging loss instead of the material hysteresis loss, dominates the system COP. This also means that for materials of comparable FOM, on the system level it is easier to transfer the high material performance to the system level because a lower external charging efficiency $\eta_{DC} < 100\%$ is sufficient to reach comparable $COP_{R,SYS} < COP_{R,MAT}$. In Fig. 3 this effect is clearly visible, where for the polymers a lower requirement for the charging efficiency is present, whereas for the ceramics (especially PMN) ultra-high external efficiencies are required to come close to the material limit.

Conclusion

High performance electrocaloric materials theoretically enable highly efficient and high power density cooling or heating through heat pumps with zero global warming potential. The heat pump system performance is reduced from the material limit due to additional losses of the charging electronics. Different electrocaloric materials (e.g. ceramics and polymers) result in significantly differing heat pump system parameters related to efficiency and power density,

which might be overlooked if only the electrocaloric material (but not a system) is studied. Especially for electrocaloric ceramics, a high charging efficiency (charge recovery efficiency) is required. Application of recently published over 99.7% efficient power electronics to electrocaloric ceramics theoretically allows to achieve over 50% of the Carnot-limit for Carnot-like thermal cycles on the system level. The combination of highly efficient and high power density electrocaloric materials with ultra-efficient power electronics (both already available today) enables to predict the feasibility of electrocaloric heat pumps with competitive performance compared to vapor compression systems. Despite these encouraging results, published electrocaloric heat pump systems today still lack significantly behind these theoretical limits and only small-scale (low temperature span or absolute cooling power) demonstrators have been published so far. However, because there are no obvious roadblocks, and the technology could enable efficient emission-free cooling and heating (if powered by renewable energies such as wind and solar), further multi-disciplinary research should be carried out in a timely manner to accelerate solving society's energy and climate crisis.

References

1. J. Shi, D. Han, Z. Li, L. Yang, S.-G. Lu, Z. Zhong, J. Chen, Q.M. Zhang, X. Qian, Electrocaloric cooling materials and devices for zero-global-warming-potential, high-efficiency refrigeration. Joule **3**(5), 1200–1225 (2019). https://doi.org/10.1016/j.joule.2019.03.021

2. U. Plaznik, M. Vrabelj, Z. Kutnjak, B. Malič, A. Poredoš, A. Kitanovski, Electrocaloric cooling: The importance of electric-energy recovery and heat regeneration. EPL (Europhysics Letters) **111**(5), 57009 (2015). https://doi.org/10.1209/0295-5075/111/57009

3. B. Neese, B. Chu, S.-G. Lu, Y. Wang, E. Furman, Q.M. Zhang, Large electrocaloric effect in ferroelectric polymers near room temperature. Science **321**(5890), 821–823 (2008). https://doi.org/10.1126/science.1159655

4. H. Johra, C. Bahl, Innovative heating and cooling systems based on caloric effects: CLIMA 2022 conference, 2022: CLIMA 2022 The 14th REHVA HVAC World Congress, (2022). https://doi.org/10.34641/CLIMA.2022.275

5. H. Johra, Performance overview of caloric heat pumps: magnetocaloric, elastocaloric, electrocaloric and barocaloric systems. (2022). https://doi.org/10.54337/aau467469997

6. S. Moench, R. Reiner, P. Waltereit, C. Molin, S. Gebhardt, D. Bach, R. Binninger, K. Bartholome, Enhancing electrocaloric heat pump performance by over 99% efficient power converters and offset fields. IEEE Access **10**, 46-571-46–588 (2022). https://doi.org/10.1109/ACCESS.2022.3170451

7. D.E. Schwartz, Thermodynamic cycles and electrical charge recovery in high-efficiency electrocaloric cooling systems. Int J Refrig (2021). https://doi.org/10.1016/j.ijrefrig.2021.02.003

8. T. Hess, L.M. Maier, P. Corhan, O. Schäfer-Welsen, J. Wöllenstein, K. Bartholomé, Modelling cascaded caloric refrigeration systems that are based on thermal diodes or switches. Int J Refrig **103**, 215–222 (2019). https://doi.org/10.1016/j.ijrefrig.2019.04.013

9. J. Schipper, D. Bach, S. Mönch, C. Molin, S. Gebhardt, J. Wöllenstein, O. Schäfer-Welsen, C. Vogel, R. Langebach, K. Bartholomé, On the efficiency of caloric materials in direct comparison with exergetic grades of compressors. J Phys.: Energy **5**(4), 045002 (2023). https://doi.org/10.1088/2515-7655/ace7f4

10. G. Suchaneck, G. Gerlach, Lead-free relaxor ferroelectrics for electrocaloric cooling. Mater. Today: Proc. **3**(2), 622–631 (2016). https://doi.org/10.1016/j.matpr.2016.01.100

11. N. Zeggai, B. Dkhil, M. LoBue, M. Almanza, Cooling efficiency and losses in electrocaloric materials. Appl. Phys. Lett. **122**(8), 081903 (2023). https://doi.org/10.1063/5.0138887

12. T. Hess, L.M. Maier, N. Bachmann, P. Corhan, O. Schäfer-Welsen, J. Wöllenstein, K. Bartholomé, Thermal hysteresis and its impact on the efficiency of first-order caloric materials. J. Appl. Phys. **127**(7), 075103 (2020). https://doi.org/10.1063/1.5132897

13. L. Zhu, Exploring strategies for high dielectric constant and low loss polymer dielectrics. J Phys. Chem. Lett. **5**(21), 3677–3687 (2014). https://doi.org/10.1021/jz501831q

14. Z. Wang, R. Zhang, E. Sun, W. Cao, Contributions of domain wall motion to complex electromechanical coefficients of 0.62Pb(Mg(13)Nb(23))O(3)-0.38PbTiO(3) crystals. J. Appl. Phys. **107**(1), 14110 (2010). https://doi.org/10.1063/1.3273484

15. A. Grünebohm, T. Nishimatsu, Influence of defects on ferroelectric and electrocaloric properties of BaTiO3. Phys. Rev. B **93**, 13 (2016). https://doi.org/10.1103/PhysRevB.93.134101

16. V.I. Sultanov, V.V. Atrazhev, D.V. Dmitriev, Combined analytical and molecular dynamics model of electrocaloric effect in poly(VDF- co- TrFE) copolymer. J. Polym. Sci. (2023). https://doi.org/10.1002/pol.20230153

17. M. Almanza, T. Martinez, M. Petit, Y. Civet, Y. Perriard, M. LoBue, Adaptation of a solid-state marx modulator for electroactive polymer. IEEE Trans. Power Electron. **37**(11), 13014–13021 (2022). https://doi.org/10.1109/TPEL.2022.3183437

18. E. Defay, R. Faye, G. Despesse, H. Strozyk, D. Sette, S. Crossley, X. Moya, N.D. Mathur, Enhanced electrocaloric efficiency via energy recovery. Nat. Commun. (2018). https://doi.org/10.1038/s41467-018-04027-9

19. Y. Meng, Z. Zhang, H. Wu, R. Wu, J. Wu, H. Wang, Q. Pei, A cascade electrocaloric cooling device for large temperature lift. Nat. Energy **5**(12), 996–1002 (2020). https://doi.org/10.1038/s41560-020-00715-3

20. X. Qian, D. Han, L. Zheng, J. Chen, M. Tyagi, Q. Li, F. Du, S. Zheng, X. Huang, S. Zhang, J. Shi, H. Huang, X. Shi, J. Chen, H. Qin, J. Bernholc, X. Chen, L.-Q. Chen, L. Hong, Q.M. Zhang, High-entropy polymer produces a giant electrocaloric effect at low fields. Nature **600**(7890), 664–669 (2021). https://doi.org/10.1038/s41586-021-04189-5

21. S. Mönch, R. Reiner, K. Mansour, P. Waltereit, M. Basler, R. Quay, C. Molin, S. Gebhardt, D. Bach, R. Binninger, K. Bartholomé, A 99.74% efficient capacitor-charging converter using partial power processing for electrocalorics. IEEE J. Emerg. Sel. Top. Power Electron. (2023). https://doi.org/10.1109/JESTPE.2023.3270375

22. P. Lheritier, A. Torelló, T. Usui, Y. Nouchokgwe, A. Aravindhan, J. Li, U. Prah, V. Kovacova, O. Bouton, S. Hirose, E. Defay, Large harvested energy with non-linear pyroelectric modules. Nature **609**(7928), 718–721 (2022). https://doi.org/10.1038/s41586-022-05069-2

23. C. Molin, P. Neumeister, H. Neubert, S.E. Gebhardt, Multilayer ceramics for electrocaloric cooling applications. Energy Technol. **6**(8), 1543–1552 (2018). https://doi.org/10.1002/ente.201800127

24. A. Torelló, E. Defay, Electrocaloric coolers: a review. Adv. Electron. Mater. (2022). https://doi.org/10.1002/aelm.202101031

25. A. Greco, C. Masselli, Electrocaloric cooling: a review of the thermodynamic cycles, materials, models, and devices. Magnetochemistry **6**(4), 67 (2020). https://doi.org/10.3390/magnetochemistry6040067

26. S. Moench, R. Reiner, K. Mansour, M. Basler, P. Waltereit, R. Quay, K. Bartholomé, "GaN Power Converter Applied to Electrocaloric Heat Pump Prototype and Carnot Cycle. In *2022 IEEE 9th workshop on wide bandgap power devices & applications (WiPDA)*, pp. 186–191. (2022). https://doi.org/10.1109/WiPDA56483.2022.9955287

27. Y. Wang, Z. Zhang, T. Usui, M. Benedict, S. Hirose, J. Lee, J. Kalb, D. Schwartz, A high-performance solid-state electrocaloric cooling system. Science **370**(6512), 129–133 (2020). https://doi.org/10.1126/science.aba2648

28. L. Shebanov, K. Borman, On lead-scandium tantalate solid solutions with high electrocaloric effect. Ferroelectrics **127**(1), 143–148 (1992). https://doi.org/10.1080/00150199208223361

29. B. Nair, T. Usui, S. Crossley, S. Kurdi, G.G. Guzmán-Verri, X. Moya, S. Hirose, N.D. Mathur, Large electrocaloric effects in oxide multilayer capacitors over a wide temperature range.

30. Nature **575**(7783), 468–472 (2019). https://doi.org/10.1038/s41586-019-1634-0

30. Y. Nouchokgwe, P. Lheritier, C.-H. Hong, A. Torelló, R. Faye, W. Jo, C.R.H. Bahl, E. Defay, Giant electrocaloric materials energy efficiency in highly ordered lead scandium tantalate. Nat. Commun. **12**(1), 3298 (2021). https://doi.org/10.1038/s41467-021-23354-y

31. J. Li, A. Torelló, Y. Nouchokgwe, T. Granzow, V. Kovacova, S. Hirose, E. Defay, Electrocaloric effect in BaTiO 3 multilayer capacitors with first-order phase transitions. J. Phys.: Energy **5**(2), 024017 (2023). https://doi.org/10.1088/2515-7655/acc972

32. Z. Li, C. Molin, S.E. Gebhardt, Influence of sintering additives on modified (Ba, Sr)(Sn, Ti)O3 for electrocaloric application. Inorganics **11**(4), 151 (2023). https://doi.org/10.3390/inorganics11040151

33. H. Cui, Q. Zhang, Y. Bo, P. Bai, M. Wang, C. Zhang, X. Qian, R. Ma, Flexible microfluidic electrocaloric cooling capillary tube with giant specific device cooling power density. Joule **6**(1), 258–268 (2022)

34. K. Klinar, A. Kitanovski, Thermal control elements for caloric energy conversion. Renew. Sustain. Energy Rev. **118**, 109571 (2020). https://doi.org/10.1016/j.rser.2019.109571

35. N. Petelin, K. Vozel, K. Klinar, A. Kitanovski, The numerical study on performance evaluation of a thermal switch capacitor in a magnetocaloric cooling device. iScience **25**(12), 105517 (2022)

36. K. Klinar, K. Vozel, T. Swoboda, T. Sojer, M. Muñoz Rojo, A. Kitanovski, Ferrofluidic thermal switch in a magnetocaloric device. iScience **25**(2), 103779 (2022)

37. L.M. Maier, P. Corhan, A. Barcza, H.A. Vieyra, C. Vogel, J.D. Koenig, O. Schäfer-Welsen, J. Wöllenstein, K. Bartholomé, Active magnetocaloric heat pipes provide enhanced specific power of caloric refrigeration. Commun. Phys. (2020). https://doi.org/10.1038/s42005-020-00450-x

38. Y. Wang, D.E. Schwartz, S.J. Smullin, Q. Wang, M.J. Sheridan, Silicon heat switches for electrocaloric cooling. J. Microelectromech. Syst. **26**(3), 580–587 (2017). https://doi.org/10.1109/JMEMS.2017.2676704

39. X.-S. Qian, H.-J. Ye, Y.-T. Zhang, H. Gu, X. Li, C.A. Randall, Q.M. Zhang, Giant electrocaloric response over a broad temperature range in modified BaTio3 ceramics. Adv. Funct. Mater. **24**(9), 1300–1305 (2014). https://doi.org/10.1002/adfm.201302386

40. T. Zhang, X.-S. Qian, H. Gu, Y. Hou, Q.M. Zhang, An electrocaloric refrigerator with direct solid to solid regeneration. Appl. Phys. Lett. **110**(24), 243503 (2017). https://doi.org/10.1063/1.4986508

41. M. Scott, Working safely with hazardous capacitors: establishing practical thresholds for risks associated with stored capacitor energy. IEEE Ind. Appl. Mag. **25**(3), 44–53 (2019). https://doi.org/10.1109/MIAS.2018.2875130